Multiconformational NMR Analysis of Sandostatin (Octreotide): Equilibrium between β-Sheet and Partially Helical Structures[†,‡]

Giuseppe Melacini, Qin Zhu,[§] and Murray Goodman*

Department of Chemistry and Biochemistry, University of California at San Diego, La Jolla, California 92093-0343

Received October 4, 1996; Revised Manuscript Received December 2, 1996[⊗]

ABSTRACT: This paper reports a detailed conformational analysis by ^{1}H NMR (DMSO-d_6, 300 K) and molecular modeling of the octapeptide D-Phe[1]-Cys[2]-Phe[3]-D-Trp[4]-Lys[5]-Thr[6]-Cys[7]-Thr[8]-ol (disulfide bridged) known as sandostatin (or SMS 201−995 or octreotide) with both somatostatin-like and opioid-like bioactivities. This is the initial report on sandostatin showing that attempts to explain all NMR data using a single average conformation reveal several important inconsistencies including severe violations of mutually exclusive backbone-to-backbone NOEs. The inconsistencies are solved by assuming an equilibrium between antiparallel β-sheet structures and conformations in which the C-terminal residues form a 3_{10} helix-like fold (helical ensemble). This conformational equilibrium is consistent with previous X-ray diffraction investigations which show that sandostatin can adopt both the β-sheet and the 3_{10} helix-like secondary structure folds. In addition, indications of a conformational equilibrium between β-sheet and helical structures are also found in solvent systems different from DMSO-d_6 and for other highly bioactive analogs of sandostatin. In these cases a proper multiconformational NMR refinement is important in order to avoid conformational averaging artifacts. Finally, using the known models for somatostatin-like and opioid-like bioactivities of sandostatin analogs, the present investigation shows the potentials of the proposed structures for the design of novel sandostatin-based conformationally restricted peptidomimetics. These analogs are expected to refine the pharmacophore models for sandostatin bioactivities.

Somatostatin is a cyclic tetradecapeptide which inhibits the release of many hormones including the growth hormone, glucagon, insulin, and gastrin (Reichlin, 1983a,b). Furthermore, somatostatin plays a role in neural transmission (Delfs & Dichter, 1983; Iverson, 1983; Seybold et al., 1983), but the possible medicinal applications of somatostatin *in vivo* are limited by its rapid proteolytic degradation (plasma half-life < 3 min) (Kaupmann et al., 1995). However, several short synthetic somatostatin analogs with increased metabolic stability have been synthesized (Bauer et al., 1982; Brady et al., 1993; Rivier et al., 1975; Veber et al., 1978, 1981), resulting in multiple therapeutic applications. For instance, the octapeptide D-Phe[1]-Cys[2]-Phe[3]-D-Trp[4]-Lys[5]-Thr[6]-Cys[7]-Thr[8]-ol (disulfide bridged) known as SMS 201−995 or sandostatin is an exceptionally potent inhibitor of growth hormone release (Bauer et al., 1982) and is used for the treatment of various endocrine and malignant disorders (Kaupmann et al., 1995). Sandostatin is also known to bind to opioid receptors (Maurer et al., 1982) and the fundamental work of Hruby et al. has shown that conformationally restricted somatostatin-like analogs can be designed on the basis of sandostatin, resulting in high potency and selectivity for the μ-opioid receptor (Pelton et al., 1985, 1986; Gulya et al., 1986; Shook et al., 1987; Kazmierski & Hruby, 1988; Kazmierski et al., 1988, 1991, 1992, 1995; Hawkins et al., 1989; Kramer et al., 1989).

The varied medicinal applications of sandostatin have made it the object of numerous structural investigations using different techniques which include nuclear magnetic resonance (NMR)[1] spectroscopy (Wynants et al., 1985a,b, 1989; Widmer et al., 1993) and X-ray diffraction (Pohl et al., 1995). The pioneering NMR studies of Van Binst et al. in water and in DMSO-d_6 solutions (Wynants et al., 1985b, 1989) have shown that sandostatin adopts a predominant antiparallel β-sheet conformation characterized by a type II′ β-like turn spanning residues D-Trp[4] and Lys[5]. Similar secondary structure features were also found for sandostatin dissolved in a water/MeOH mixture (Widmer et al., 1993) and for one of the molecules in the asymmetric unit of sandostatin crystals (molecule I; see ribbon structure representation in Figure 1a) (Pohl et al., 1995). The asymmetric unit also contains two other sandostatin molecules (II and III) in which the conformation of residues D-Phe[1]−Lys[5] is similar to that observed for molecule I but the C-terminal tripeptide folds into a helical array (see ribbon structure representations in Figure 1b,c) (Pohl et al., 1995). The folded conformation of the X-ray structures II and III is stabilized by the Cys[7] NH−D-Trp[4] C═O and by the Phe[3] NH−Thr[6] H−O hydrogen bonds (Pohl et al., 1995). This helical fold has not been reported in other sandostatin structure determinations.

This paper is the first report on sandostatin showing that the commonly proposed antiparallel β-sheet structure of

† This work was supported by the National Institutes of Health (Grant DK 15410).

‡ Coordinates have been deposited in the Brookhaven Protein Data Bank under file name 1SOC.

* To whom correspondence should be addressed.

§ Present address: Department of Biochemistry, Purdue University, West Lafayette, IN 47907.

⊗ Abstract published in *Advance ACS Abstracts,* January 15, 1997.

[1] Abbreviations: DG, distance geometry; DMSO-d_6, fully deuterated dimethyl sulfoxide; DQF-COSY, double-quantum-filtered correlation spectroscopy; $J_{C^\alpha HC^\beta H}$, coupling constant between the $C^\alpha H$ and the $C^\beta H$ protons; $J_{HNC^\alpha H}$, coupling constant between the NH and the $C^\alpha H$ protons; MD, molecular dynamics; MeOH, methanol; NOE, nuclear overhauser enhancement; NMR, nuclear magnetic resonance; ROESY, rotating frame nuclear Overhauser spectroscopy; Tic, 1,2,3,4-tetrahydroisoquinolinecarboxylic acid; TOCSY, total correlation spectroscopy.

S0006-2960(96)02497-X CCC: $14.00

sandostatin explains some of the NMR data acquired in DMSO-d_6 solution but cannot account for all the observed NOEs and temperature coefficients. In addition, discrepancies are found between some NOEs and the $J_{HNC^{\alpha}H}$ coupling constants. These inconsistencies are eliminated if a conformational equilibrium is considered between the two secondary structures observed in sandostatin crystals. Clear evidence for this conformational equilibrium is also found in other solvent systems and for other highly bioactive molecules closely related to sandostatin. The biological relevance of this conformational equilibrium is also considered in view of the somatostatin-like and opioid-like bioactivities of sandostatin. For these bioactivities, pharmacophore models were previously proposed on the basis of structure−activity studies of conformationally constrained analogs (Schiller & Di Maio, 1982; Pelton et al., 1985, 1986, 1988; Kazmierski & Hruby, 1988; Kazmierski et al., 1988, 1991, 1992, 1995; Schiller, 1988; Sugg et al., 1988; Hawkins et al., 1989; Kramer et al., 1989; Mierke et al., 1990a,b; Schiller et al., 1991, 1992; Yamazaki et al., 1991a, 1992; Huang et al., 1992; He et al., 1993).

MATERIALS AND METHODS

NMR Spectroscopy. The sample (generously provided by Sandoz) was dissolved in DMSO-d_6 and then lyophilized (purchased from Merck Sharp and Dohme Canada Ltd). The dry sample was redissolved in DMSO-d_6 at concentrations approximately 6 mM and degassed by the freeze−pump−thaw method. All ^{1}H NMR spectra were measured on a Bruker AMX 500 spectrometer operating at 500 MHz. The one-dimensional spectra contain 16K data points with a spectral width of 6500 Hz. The 1D spectra were acquired at temperatures between 300 and 320 K and were used to measure the amide resonance temperature coefficients. The 2D spectra were acquired at 300 K. The total correlation spectroscopy (TOCSY) experiments were performed using the MLEV-17 sequence and the time-proportional phase increment (Bax & Davis, 1980; Bodenhausen et al., 1980; Davis & Bax, 1985; Levitt et al., 1982). A mixing time of 75 ms with a spin-locking field of 10 kHz was employed. The rotating frame nuclear Overhauser (ROESY) experiments (Bothner-By et al., 1984) were carried out with mixing times of 100, 200, and 300 ms. A spin-locking field of 2.5 kHz was used. The TOCSY and ROESY experiments were obtained using 2K data points in the f_2 domain and 256 points in the f_1 domain. Zero-filling was applied in the f_1 and f_2 domains to obtain a matrix of 2K × 2K data points. The DQF-COSY experiment (Aue et al., 1976; Bax & Freeman, 1981; Rance et al., 1984; Shaka & Freeman, 1983) was acquired using 4K data points in the f_2 domain in order to have higher digital resolution. Multiplication with a phase-shifted sine-bell function was employed to enhance the spectra.

The NMR spectra were processed using FELIX (Biosym/MSI, Inc.). Chemical shifts were measured using DMSO-d_6 ($\delta = 2.49$ ppm) as an internal standard. (See Supporting Information for the assignments.) The observed signals of nonoverlapping $C^{\beta}H$ resonances were stereospecifically assigned to their respective $C^{\beta}H$ protons following the procedures described by Yamazaki et al. (1991b) and Zuiderweg et al. (1985). The $J_{HNC^{\alpha}H}$ and $J_{C^{\alpha}HC^{\beta}H}$ coupling constants were obtained by 1D spectra and by sections of cross peaks from the resolution-enhanced 4K × 2K DQF-COSY spectrum. The ROESY cross peak volumes were calibrated against the distance between the indole and H2 protons of D-Trp[4] using the isolated spin pair approximation (Noggle & Schirmer, 1971). On the basis of the comparison with other known distances (Pepermans et al., 1988), an error of approximately ±0.5 Å was estimated. Consequently, the upper and lower distance constraints were set to the measured distance ±0.5 Å, respectively.

Molecular Modeling. The structural NMR refinement protocol included distance geometry, energy minimizations, restrained simulated annealing, and cluster analysis. The distance geometry (DG) program (DGII, Biosym Technologies, Inc.) was used to generate structures consistent with the distance constraints derived from NOEs. The ϕ torsional angles and hydrogen-bonding patterns of these structures were compared with the values derived from NMR measurements. A Karplus-type equation was used (Bystrov, 1976) to compute the ϕ torsion values, consistent with the measured $J_{HNC^{\alpha}H}$ coupling constants, and an error of ±30° was tolerated at this stage of the refinement. In the case of the hydrogen bond based selection, structures were retained in which the NH protons with an absolute value of the temperature coefficient <2 ppb/K (Kessler, 1982) donate at least one hydrogen bond, fulfilling the loose thresholds of 3.0 Å and 110° for the NH proton−acceptor distance and for the angle defined by three atoms, N−H−oxygen of the acceptor carbonyl, respectively (Baker et al., 1984). Structures which did not fulfill these requirements were discarded. The remaining structures were subjected to a restrained simulated annealing protocol.

Molecular dynamics (MD) and mechanics calculations were carried out *in vacuo* employing, the DISCOVER program (Hagler, 1985; Biosym/MSI, Inc.) with the CVFF force field, and the NOE restraints were included with a force constant of 15 kcal/(mol Å^2). A distance-dependent dielectric constant was used to take into account the solvent effects (McCammon et al., 1979). A neutral form of the amine group in the Lys side chain was used in order to be consistent with previous studies (Huang et al., 1992). A harmonic bond stretching potential was used. This prevented the bonded atoms from drifting unrealistically far apart because of high-energy nonbonded interactions. During all the simulations no cross terms were used because no normal mode analysis was attempted. In all simulations the peptide bonds were kept in the *trans* structure.

Prior to every molecular dynamics simulation the system was equilibrated with 3 ps initialization dynamics. In an attempt to carry out a thorough search of the accessible conformational space, the selected distance geometry structures were first submitted to 10 ps of molecular dynamics at 1000 K with a step size of 1 fs. At regular intervals of 1 ps, conformations were extracted and submitted to a preliminary energy minimization by steepest descent until the maximum derivative was less than 1. Starting from each of these minimized conformations, we proceeded with 10 ps of molecular dynamics at 300 K. Again, at regular intervals of 1 ps, we carried out unrestrained minimizations to generate families of low-energy conformations. For these minimiza-

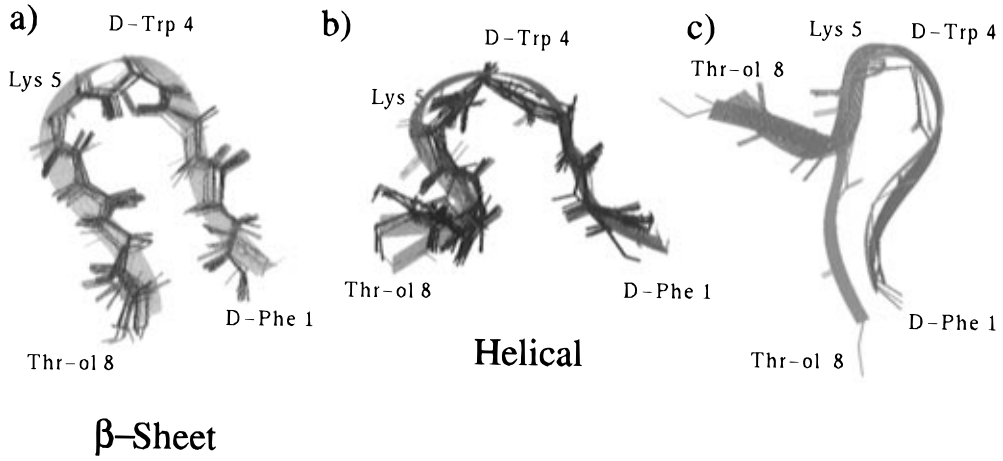

FIGURE 1: Backbones of sandostatin. (a) Black: structures obtained from the NMR data using a traditional refinement protocol which attempts to fit all the data with a single conformation. Green: backbone and ribbon of one of the three molecules found in the asymmetric unit of sandostatin crystals (Pohl et al., 1995). The X-ray-derived structure of this molecule, denoted as molecule I by Pohl et al., will be referred to here as X-ray structure I. Similarly, the X-ray-derived structures of molecules II and III (Pohl et al., 1995) will be denoted here as X-ray structures II and III, respectively. The backbone rmsd between the β-sheet NMR structures and the X-ray structure I is in the range 0.716−1.429 Å. (b) Black: representative conformations found in the 500 ps molecular dynamics trajectories run at 300 K starting from the minimized X-ray structures II and III (Pohl et al., 1995). A 10 kcal/mol energy cutoff is used and every conformation represents a snapshot recorded every 10 ps and minimized. Red: backbone and ribbon of the X-ray structures II and III. (c) A different view of the same X-ray structures also shown in parts a and b. The same color coding as in parts a and b is used. In the region including residues 1−5 the backbone rmsd is 0.565 and 0.696 Å for the structure pairs I−II and I−III, respectively; however, the X-ray structures II and III (red) differ from the X-ray structure I (green) in the C-terminal region: the Thr^6-Cys^7-Thr^8-ol residues adopt an extended conformation in the X-ray structure I while they form a helical fold in the X-ray structures II and III.

tions the VA09A algorithm was used until the maximum derivative was less than 0.01 kcal/mol.

The simulated annealing protocol led to 100 minimized conformations per each structure selected after distance geometry. The resulting conformations were then examined and selected according to their consistency with the $J_{HNC^{\alpha}H}$ coupling constants and the temperature coefficients. Deviations less than 20° were tolerated for any single ϕ torsion estimated from the $J_{HNC^{\alpha}H}$ coupling constants. For the temperature coefficients the selection criteria used after DG were applied but with a more restrictive threshold of 2.6 Å for the NH proton−acceptor distance (Baker et al., 1984). Those structures consistent with the experimental values and with energies not higher than 10 kcal/mol compared to the lowest energy were selected (Kazmierski et al., 1995). No violation was detected for the lower limits of the distance constraints. The agreement of the final selected structures with the distance upper limits derived from the NOEs was analyzed as discussed in the following section.

Additional structures were generated via molecular dynamics starting from the three minimized X-ray structures of sandostatin (molecules I−III) (Pohl et al., 1995): prior to molecular dynamics, hydrogens were added to the X-ray structures using InsightII (Biosym/MSI, Inc.); the potentials and charges were then assigned according to the CVFF force field; a distance-dependent dielectric constant (McCammon et al., 1979) and a neutral form of the amine group in the Lys side chain were used consistently with the settings chosen in the NMR refine protocol; the resulting structures were minimized using the VA09A algorithm. These minimized X-ray structures were submitted to 500 ps of unrestrained molecular dynamics at 300 K during which structures were extracted and minimized at regular intervals of 10 ps using the same procedure described above for the simulated annealing protocol.

RESULTS AND DISCUSSION

The Backbone

The Monoconformational Approach (One-State Model). The simplest approach to the conformational analysis of peptides relies on the use of a single conformation to explain all the NMR data available, including all NOEs, coupling constants, and information on the NH proton shielding. We therefore used a combined distance geometry and molecular dynamics protocol to search for structures of sandostatin consistent with our experimental data acquired in DMSO-d_6 at 300 K. This monoconformational approach led to a family of structures which converged: the backbone rmsd to the mean structure is 0.489 ± 0.139 Å, comparable to the convergence obtained for structurally well-defined proteins (Clore et al., 1990). This NMR-based conformation family is very similar to the X-ray-based structure of one of the molecules found in the asymmetric unit of sandostatin crystals (molecule I, Figure 1a) (Pohl et al., 1995). In addition, a similar conformation was previously proposed for sandostatin on the basis of a qualitative structural analysis of the NMR data acquired in DMSO-d_6 at 303 K (Wynants et al., 1985b).

Both the X-ray structure I and the family of conformations coming from the monoconformational NMR refinement are characterized by an antiparallel β-pleated sheet with a type II′ β-like turn spanning residues D-Trp^4 and Lys^5 and stabilized by the Thr^6 NH−Phe^3 C═O hydrogen bond. This turn is supported by the strong D-Trp^4 C$^{\alpha}$H−Lys^5 NH NOE, by the medium Lys^5 NH−Thr^6 NH NOE (Table 1), and by the low-temperature coefficient measured for the Thr^6 NH resonance (0.6 −ppb/K). The extended conformation found for the other parts of the backbone is supported by the sequence of strong sequential C$^{\alpha}$H−NH NOEs (Table 1) and of high (>8 Hz) $J_{HNC^{\alpha}H}$ coupling constants (Table 2). In addition, the high-temperature coefficients measured for the

Table 1: Backbone NOEs of Sandostatin (Violated NOEs Are Underlined)

	NOE[b]	exptl[c] (Å)	NOE violations[a] (%) β-sheet[d]	helical[e]
1	Cys^2 $C^\alpha H-Phe^3$ NH	2.7	0	0
2	Cys^2 $C^\alpha H-Cys^7$ $C^\alpha H$	4.0[f]	0	81
3	Phe^3 $C^\alpha H-$D$-Trp^4$ NH	2.4	0	0
4	D$-Trp^4$ $C^\alpha H-Lys^5$NH	2.5	0	0
5	D$-Trp^4$ $C^\alpha H-Thr^6$ NH	4.6[f]	0	0
6	Lys^5 NH$-Thr^6$NH	3.1	0	3
7	Lys^5 $C^\alpha H-Cys^7$ NH	4.9[f]	3	0
8	Thr^6 $C^\alpha H-Cys^7$ NH	2.6	0	83
9	Thr^6 NH$-Cys^7$ NH	3.9	86	0
10	Thr^6 $C^\alpha H-Thr^8$ NH	4.7[f]	100	0
11	Cys^7 $C^\alpha H-Thr^8$ NH	2.7	0	60
12	Cys^7 NH$-Thr^8$ NH	3.6	100	0
13	Cys^7 $C^\alpha H-Phe^3$ NH	4.6[f]	0	92

[a] Violations are reported as percentages of structures with distances larger than the experimental upper limit (Kessler et al., 1988). NOEs with nonrestraining upper limits are not reported. [b] NOEs involving Cys^2 NH are not accessible. [c] Experimental upper limits were obtained from 500 MHz ROESY spectra in DMSO-d_6 at 300 K, unless otherwise specified. [d] Structures are from traditional monoconformational NMR refinement and are similar to the X-ray structure I (Pohl et al., 1995). [e] Conformations are from 500 ps molecular dynamics trajectories at 300 K starting from X-ray structures II and III (Pohl et al., 1995). The NOE between protons i and j is considered violated when $r_{eff}(i,j) > r_{exptl}(i,j)$, where $r_{eff}(i,j) = \langle r_{ij}^{-3}\rangle^{-1/3}$ (Kessler et al., 1988) and $r_{exptl}(i,j)$ is the experimentally measured upper limit. Both trajectories resulted in the same NOE violations. [f] This NOE is not resolved in our spectra of sandostatin in DMSO-d_6 solution but is resolved in the NOESY spectra of sandostatin in H_2O/MeOH-d_4 (5.7:1 v/v) (Widmer et al., 1993).

Table 2: Coupling Constants $^3J_{HNC^\alpha H}$ (in Hz) of Sandostatin in DMSO-d_6 at 300 K

residue[a]	exptl $^3J_{HNC^\alpha H}$[b]	calcd $^3J_{HNC^\alpha H}$[c] β-sheet[d]	helical[d]
Phe^3	8.8	8.2−10.7	8.7 ± 1.8
D-Trp^4	4.7	3.5−5.1	6.4 ± 2.4
Lys^5	8.8	5.5−9.7	5.9 ± 2.8
Thr^6	8.1	7.4−9.6	5.4 ± 2.6
Cys^7	8.5	8.2−10.5	6.8 ± 3.0
Thr^8	8.8	6.1−8.6	8.2 ± 2.0

[a] The $^3J_{HNC^\alpha H}$ involving Cys^2 NH is not accessible. [b] Experimental value. [c] The $^3J_{HNC^\alpha H}$ coupling constants are calculated using the Karplus equation $^3J_{HNC^\alpha H} = A\cos^2|\phi \pm 60°| + B\cos|\phi \pm 60°| + C$, with $A = 9.4$, $B = -1.1$ and $C = 0.4$ (Bystrov, 1976). The (+) is for a D-configuration and the (−) is for an L-configuration. In the case of the β-sheet conformational family it is difficult to estimate reliably the relative weight of every single conformation because a distance geometry algorithm was used and it does not contain a physically meaningful force field. In addition, J values are rapidly changing functions of the torsion angle. Therefore, we took the conservative approach of reporting only the minimum and maximum calculated $^3J_{HNC^\alpha H}$ values within the β-sheet structural family. This problem does not exist for the helical ensemble which results only from molecular dynamics runs. In this case we report the average $^3J_{HNC^\alpha H}$ value ± the standard deviation. [d] See Table 1.

D-Trp^4 and Cys^7 NH resonances (6.5 and 8.1 −ppb/K, respectively) are fully consistent with the solvent exposure expected for these protons in the antiparallel β-sheet structure (Figure 1a).

The consistency with the above-mentioned NMR data and the similarity to the X-ray structure I (Pohl et al., 1995) of sandostatin show the importance of the monoconformational NMR refinement. However, the β-sheet conformational family obtained by this approach cannot by itself explain all the observed NMR data as demonstrated below.

The Insufficiency of the One-State Model. Several inconsistencies show that the one-state model described above is not sufficient to account for all the available experimental data:

(a) The sequential Thr^6 NH−Cys^7 NH and Cys^7 NH−Thr^8 NH NOEs indicative of folded structures (Wuthrich, 1986) are consistently violated by the β-sheet conformations (Table 1, NOEs 9 and 12). Conversely, the strong sequential Thr^6 $C^\alpha H-Cys^7$ NH and Cys^7 $C^\alpha H-Thr^8$ NH NOEs are consistent with the β-sheet structures (Table 1, NOEs 8 and 11) but are violated by folded conformations (Wuthrich, 1986). The NOE couple Thr^6 $C^\alpha H-Cys^7$ NH, Cys^7 $C^\alpha H-Thr^8$ NH and the NOE couple Thr^6 NH$-Cys^7$ NH, Cys^7 NH$-Thr^8$ NH (Table 1) are therefore mutually exclusive.

(b) The folded structures supported by the two sequential NH−NH NOEs mentioned in point a are not consistent with the extended average conformation indicated by the sequence of high (>8 Hz) $J_{HNC^\alpha H}$ coupling constants (Table 2).

(c) The high-temperature coefficient of Phe^3 NH (−6.3 ppb/K) indicates (Kessler, 1982) that this proton is solvent exposed while the β-sheet conformations predict it to be hydrogen bonded with Thr^6 C═O (the $NH^3-O{=}C^6$ distance is 2.0 ± 0.1 Å, the N−H−O angle is 159.9 ± 13.7°, and the H−O═C angle is 145.9 ± 5.5°).

The simultaneous observation of mutually exclusive NOEs (point a) and the discrepancies observed among the structures derived from the NOEs, the $J_{HNC^\alpha H}$ based structures (point b), and the temperature coefficient based structures (point c) are typical indications that it is not correct to interpret all the NMR data in terms of a single average conformation (Kessler et al., 1988) and led us to hypothesize a conformational equilibrium between the β-sheet structural cluster and a second conformational ensemble involving folded structures for the C-terminal residues where the inconsistencies are observed. For this purpose we considered the X-ray structures of molecules II and III found in sandostatin crystals (Pohl et al., 1995).

The Helical Ensemble. A close inspection of the X-ray structures II and III shows that the conformation in the region including residues D-Phe^1−Lys^5 is similar to that found in the X-ray structure I, while the C-terminal residues of molecules II and III adopt a helical conformation not found in the β-sheet structure of molecule I (Figure 1b,c): in molecule III residues Lys^5−Thr^8 form a 3_{10} helix [the backbone rmsd from an ideal 3_{10} helix with $(\phi, \psi) = (-60°, -30°)$ is 0.275 Å], and the conformation of molecule II is very similar to that of molecule III (backbone rmsd = 0.566 Å), the only difference arising from a flip of the $C(O)^7-NH^8$ peptide bond (Pohl et al., 1995). This type of conformational change is known to occur in peptides (Kessler et al., 1988; Kopple et al., 1986), and in the case of sandostatin it results in a significant difference of the ψ torsion of Cys^7 between the X-ray structures II and III, while all the other backbone torsions do not vary significantly (variations less than 30°). A similar behavior is found in the molecular dynamics trajectories starting from the minimized X-ray structures II and III: the three N-terminal residues adopt a backbone conformation similar to that found in the β-sheet conformational cluster; the type II′ β-like turn around D-Trp^4 and Lys^5 is also maintained (Table 3 and Figure 1b); the backbone torsions of residues Lys^5 and Thr^6 and ϕ^7 remain close to the values typical of a 3_{10} helix (Table

Table 3: Backbone Torsions of the Two Sandostatin Structural Clusters Involved in the Conformational Equilibrium[a]

residue	torsion	β-sheet[b]	helical[b]
D-Phe[1]	ψ	49 ± 30	80 ± 79[c]
Cys[2]	ϕ	−127 ± 31	−92 ± 16
	ψ	97 ± 7	94 ± 7
Phe[3]	ϕ	−121 ± 21	−154 ± 5
	ψ	94 ± 6	109 ± 15
D-Trp[4]	ϕ	65 ± 3	76 ± 3
	ψ	−119 ± 3	−105 ± 17
Lys[5]	ϕ	−77 ± 6	−74 ± 10
	ψ	−21 ± 14	−26 ± 29
Thr[6]	ϕ	−88 ± 10	−70 ± 24
	ψ	89 ± 5	−57 ± 20
Cys[7]	ϕ	−130 ± 20	−84 ± 18
	ψ	117 ± 13	31 ± 49[d]
Thr[8]	ϕ	−160 ± 4	−149 ± 12

[a] Torsions are in degrees and are reported as average ± standard deviation. [b] See Figure 1 and its caption. [c] The large standard deviation is caused by the conformational transition discussed in Figure 4. [d] The large standard deviation is caused by the conformational transition discussed in Figure 2.

3 and Figure 1b) while ψ^7 interconverts between values close to those observed for the X-ray structures II and III (Figure 2).

The Multiconformational Approach (Two-State Model). The similarity between the structures obtained by the molecular dynamics run at 300 K starting from the minimized X-ray conformations II and III (helical ensemble) and the X-ray structures II and III suggests that their secondary structure fold is not simply the result of crystal packing forces. Therefore, we considered the helical ensemble as a candidate for the equilibrium with the previously discussed β-sheet conformations. The conformational equilibrium between the β-sheet and the helical structures (multiconformational approach; Figure 1a,b) solves all the inconsistencies encountered using the monoconformational NMR refinements:

(a) Unlike the β-sheet structural family, the helical conformations violate the strong Thr[6] C$^\alpha$H−Cys[7] NH and Cys[7] C$^\alpha$H−Thr[8] NH NOEs (NOEs 8 and 11 of Table 1) as expected for folded structures, but they do not violate the Thr[6] NH−Cys[7] NH and the Cys[7] NH−Thr[8] NH NOEs (NOEs 9 and 12 of Table 1) which are violated by the β-sheet structures. Therefore, the two-state conformational equilibrium between the β-sheet and the helical structures explains (Bruschweiler et al., 1991) all observed NOEs (Table 1) including the mutually exclusive couples of NOEs Thr[6] C$^\alpha$H−Cys[7] NH, Cys[7] C$^\alpha$H−Thr[8] NH and Thr[6] NH−Cys[7] NH, Cys[7] NH−Thr[8] NH. In addition, all the other NOEs expected on the basis of the β-sheet/helical equilibrium were also checked and found to be consistent with the NMR data in DMSO-d_6 at 300 K. Some NOEs which could not be unambiguously resolved in our experimental conditions were observed in a water/MeOH-d_4 mixture (Widmer et al., 1993) (NOEs 2, 5, 7, 10, and 13 of Table 1). As shown by Table 1, the long-range Cys[2] C$^\alpha$H−Cys[7] C$^\alpha$H NOE 2 and the C$^\alpha$HNH($i + 4$, i) NOE 13 are typical of antiparallel β-sheet structures, while the C$^\alpha$HNH(i, $i + 2$) NOE 10 is typical of the 3_{10} helix-like ensemble. The simultaneous observation of these mutually exclusive NOEs provides further support for the equilibrium between the β-sheet and the helical conformations. Furthermore, the backbone structures proposed for sandostatin in DMSO-d_6 at 300 K also fit all the remaining NMR data acquired in the water/MeOH mixture (Widmer et al., 1993), suggesting that the change of experimental conditions does not significantly affect the backbone conformation.

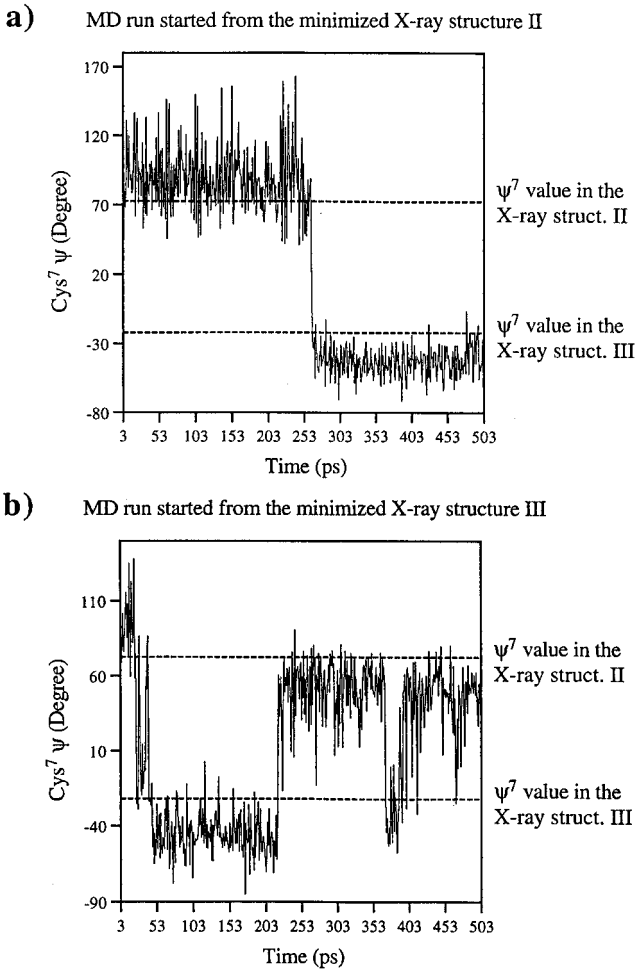

FIGURE 2: ψ backbone torsion of Cys[7] during a 500 ps time course of molecular dynamics at 300 K starting from the minimized X-ray structures II (a) and III (b) (Pohl et al., 1995), respectively. Values of ψ^7 are recorded every picosecond after equilibration of the MD runs. In both cases (a and b) a transition is observed between values close to those of the two X-ray structures considered (see dashed lines). These transitions correspond to flippings of the C(O)[7]−NH[8] peptide bond.

(b) The equilibrium between the β-sheet and the helical structures is also consistent with the observed $J_{HNC^\alpha H}$ coupling constants which are in the range of the computed $J_{HNC^\alpha H}$ coupling constants (Table 2). The coupling constants do not permit a reliable quantitative estimation of the relative β-sheet/helical populations, but the $J_{HNC^\alpha H}$ coupling constants of Thr[6] and Cys[7] adopt different values in the β-sheet and helical conformations (Table 2), and comparison with the experimental values indicates (Kessler et al., 1988) that the β-sheet cluster is the major conformational family. This finding is consistent with previous reports by Van Binst et al. which describe the β-sheet structure as the predominant conformation of sandostatin in DMSO-d_6 solution (Wynants et al., 1985b).

(c) In the helical structures, the Phe[3] NH−Thr[6] C=O hydrogen bond is broken (the NH[3]−O=C[6] distance is 5.5 ± 0.6 Å with a minimum value of 3.8 Å), explaining the high-temperature coefficient of Phe[3] NH (−6.3 ppb/K).

Table 4: Side Chain χ^1 Rotamers and $J_{C^\alpha HC^\beta H}$ Coupling Constants of Sandostatin[a]

residue	χ^1 rotamers from modeled structures[b]		$J_{C^\alpha HC^\beta Hl}$ (Hz)[d]	$J_{C^\alpha HC^\beta Hh}$ (Hz)[d]	χ^1 rotamers from $J_{C^\alpha HC^\beta H}$[e]
	β-sheet[c]	helical[c]			
D-Phe[1]	***t***, g^-, g^+	***t***	4.61	8.80	0.51, 0.39, 0.10
Cys[2]	*t*, g^- [f]	***t***			
Phe[3]	*t*, g^- [g]	***t***	8.80	8.80	0.50, 0.50, 0.00
D-Trp[4]	***t***	***t***	8.80	6.52	0.51, 0.20, 0.29
Lys[5]	***g***$^-$	***t***	4.34	11.60	0.16, 0.82, 0.02
Thr[6]	***g***$^+$	***g***$^+$	5.49		0.26[h]
Cys[7]	*t*, g^- [f]	g^-, ***g***$^+$			
Thr[8]	*t*, g^- [i]	g^-, g^+ [i]	5.80		0.29[h]

[a] Data are measured in DMSO-d_6 solution at 300 K. [b] The most populated side chain rotamer in each conformational family is marked in bold. [c] See Figure 1 for the definition of the β-sheet and helical backbone conformations. The β-sheet family is expected to be more populated (see text). [d] The subscripts *l* and *h* denote low- and high-field resonances, respectively. [e] The $J_{C^\alpha HC^\beta H}$ coupling constants were analyzed using the three-state rotamer approximation. Rotamer populations were calculated using $J_T = 13.56$ Hz and $J_G = 2.60$ Hz for nonaromatic side chains (Pachler, 1964), while for aromatic side chains $J_T = 13.85$ Hz and $J_G = 3.55$ Hz (Cung & Marraud, 1982). [f] The degeneracy of the C^β resonances of Cys[2,7] does not allow us to obtain enough conformational constraints to determine reliably the populations of these rotamers. [g] For Phe[3] the differences between the *t* and g^- populations is not significant. [h] Because the Thr residue has a single β proton, only the g^- population can be calculated while the *t* and g^+ populations cannot be distinguished. [i] Thr[8]-ol is a nonstandard amino acid, and therefore no reliable side chain populations can be estimated using molecular modeling based on a standard amino acid force field.

The Side Chains—Major χ^1 Rotamers

In Table 4 the χ^1 rotamers found for the β-sheet and the helical conformations are reported along with the χ^1 rotamer populations estimated using the $J_{C^\alpha HC^\beta H}$ coupling constants (Cung & Marraud, 1982; Pachler, 1964; Yamazaki et al., 1991b). Considering that the β-sheet structures account for the majority of the conformations in solution, it can be seen that the χ^1 rotamers predicted to be dominant in the modeled structures are consistent with the most populated χ^1 rotamers predicted by the $J_{C^\alpha HC^\beta H}$ coupling constants. These χ^1 rotamers affect the basic pharmacophore array of sandostatin and are important in obtaining insight into the biological relevance of the proposed conformations.

The Biological Significance of the Accessible Conformations

Background. As discussed above, the backbone conformational equilibria found for sandostatin in DMSO-d_6 are also consistent with the NMR data acquired in a H_2O/MeOH-d_4 (5.7:1 v/v) mixture (Widmer et al., 1993). In addition, similar conformations are found in sandostatin crytals derived from a 0.2 M aqueous oxalic acid solution and containing 52 water molecules in the asymmetric unit (Pohl et al., 1995). However, the conformations accessible to biologically active ligands in solution are not necessarily the same as those adopted by the same ligands when bound to their receptors (Loosli et al., 1985; Weber et al., 1991; Fesik et al., 1990, 1991). Despite this limitation, it is instructive to check which conformations found in solution result in pharmacophore arrays consistent with the known topographical models for specific bioactivities. This type of comparison cannot be used directly to predict the affinity of a specific conformation of a flexible ligand for a specific receptor but offers a structural basis for the design of new peptidomimetics in which selected conformations are stabilized via chemical modifications. The structural preferences of the constrained peptidomimetics are less dependent on the environment and can therefore be used as conformational probes to map the receptor binding pocket and further refine pharmacophore models for the ligands. With this perspective in mind, we examined the proposed conformations for sandostatin in relation to the known pharmacophore topographic models for somatostatin and opioid receptors.

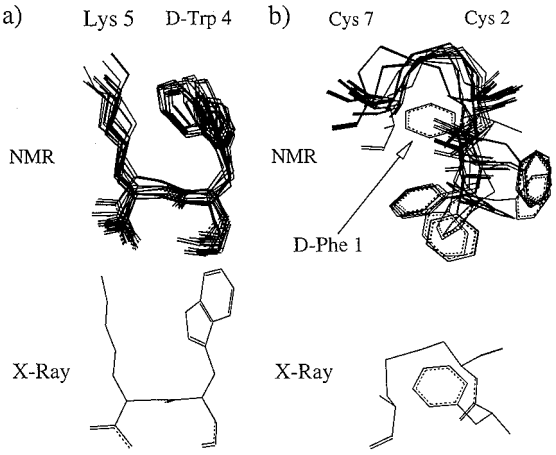

FIGURE 3: Conformations of selected side chains of sandostatin. The heavy atom representation is shown for the β-sheet structural cluster. (a) Top: "active" region including D-Trp[4] and Lys[5]. Bottom: same region in the X-ray structure I (Pohl et al., 1995) showing the similarity with the NMR-derived χ^1 rotamers, *t* for D-Trp and g^- for Lys[5]. (b) Top: "bridging" region including the disulfide-linked Cys[7] and Cys[2] and D-Phe[1]. Bottom: same region in the X-ray structure I (Pohl et al., 1995) showing the similarity with the NMR-based structure indicated by the arrow.

Somatostatin-like Bioactivity. Sandostatin is known to elicit somatostatin-like (Bauer et al., 1982) bioactivity, and the somatostatin pharmacophore model includes specific conformational constraints on the side chains of D-Trp[4] and Lys[5] revealed by the synthesis and conformational analysis of main chain and side chain chiral methylated somatostatin analogs (Huang et al., 1992). Specifically, the *t* and g^- χ^1 rotamers of D-Trp[4] and Lys[5], respectively, are expected to fit the somatostatin pharmacophore model. These rotamers are found in the β-sheet conformational family (Table 4) and allow a close proximity between the D-Trp[4] and Lys[5] side chain as confirmed by the upfield shift observed for the Lys[5] $C^\gamma H_2$ resonances and caused by the D-Trp[4] aromatic ring current (Arison et al., 1978; Buffington et al., 1980; Hallenga et al., 1980; Wynants et al., 1985b). The same χ^1 rotamers of D-Trp[4] and Lys[5] are also found in molecule I of the sandostatin crystal (Figure 3a) (Pohl et al., 1995).

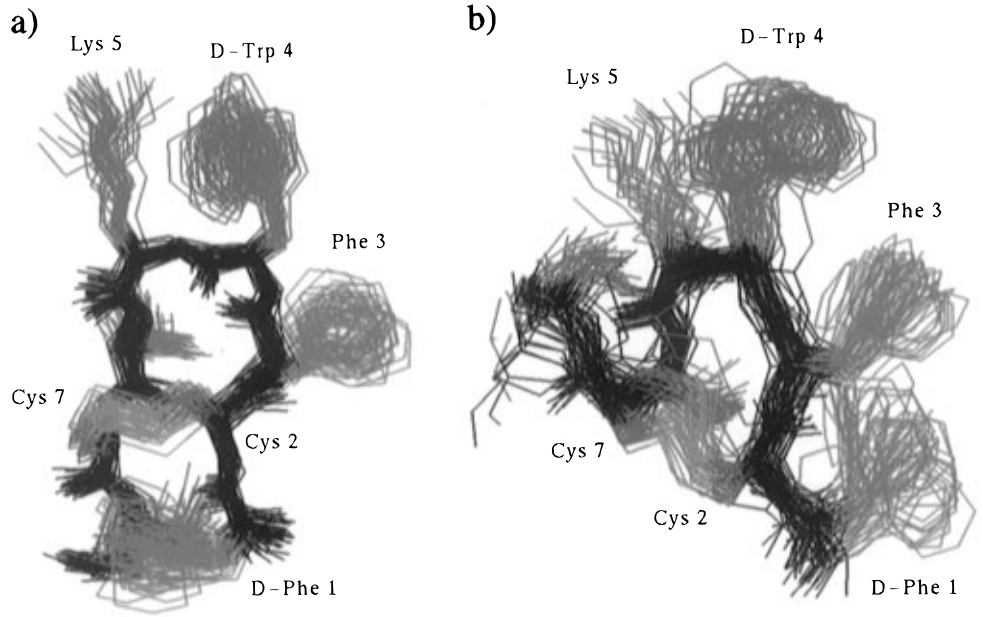

FIGURE 4: Heavy atom representations of sandostatin snapshots taken every 10 ps during a 500 ps molecular dynamics run at 300 K showing the different orientations of the D-Phe[1] side chain (green) relative to the disulfide bridge (orange) and to the Phe[3] side chain (green). All other atoms are in black (backbone) and blue (side chains). (a) Molecular dynamics run starting from the minimized X-ray structure I (Pohl et al., 1995). The D-Phe[1] side chain remains in the vicinity of the disulfide bridge. (b) Molecular dynamics run starting from the minimized X-ray structure II (Pohl et al., 1995). No conformation with the D-Phe[1] side chain close to the disulfide bridge is shown. Within the first 10 ps of molecular dynamics the D-Phe[1] side chain moves away from the disulfide bridge and approaches the Phe[3] side chain.

The somatostatin pharmacophore model also includes hydrophobic moieties, such as aromatic or disulfide groups, at approximately 9 Å from both the D-Trp[4] and the Lys[5] side chains (Huang et al., 1992; Brady et al., 1993). The side chain-to-side chain $C^{\gamma}-C^{\gamma}$ distances are employed, and in the case of the disulfide the midpoint of the S−S bond is used. This requirement is fulfilled by the β-sheet conformations in which the distances of approximately 9 Å between the disulfide bridge and the D-Trp[4] and Lys[5] side chains are accessible. Further support for the importance of the β-sheet conformations for somatostatin-like bioactivity is provided by sandostatin analogs in which the stabilization of the β-sheet structure via chemical modifications results in increased somatostatin-like bioactivity (Van Binst et al., 1992).

Opioid-like Bioactivity. Opioid receptors are known to recognize sandostatin-like ligands through interactions with their N-terminal residues. The relative orientations of the D-Phe[1] and Phe[3] side chains are expected to affect the affinities for the different opioid receptor systems (Kazmierski et al., 1995; Mierke et al., 1990a,b; Yamazaki et al., 1991a, 1992; Schiller et al., 1992a,b; Schiller, 1988; Schiller & Di Maio, 1982). The elegant structure−activity studies of Hruby et al. based on the incorporation of conformationally constrained amino acids such as Tic (1,2,3,4-tetrahydroisoquinolinecarboxylic acid) in positions 1 and 3 of sandostatin analogs (Pelton et al., 1986; Kazmierski & Hruby, 1988; Kazmierski et al., 1988, 1991, 1992, 1995; Hawkins et al., 1989; Kramer et al., 1989) have shown that two aromatic rings at a center-to-center distance of about 7.5 Å are required for high μ-opioid receptor affinity of sandostatin-based antagonists. It was also noted that two sandostatin analogs which are μ-antagonists are characterized by a left-handed disulfide bridge chirality while a third compound with different backbone conformation and right-handed disulfide bridge chirality has reduced potency as μ-opioid antagonist (Pelton et al., 1988; Sugg et al., 1988; Wynants et al., 1989).

In the case of the β-sheet structures of sandostatin the conformation of the disulfide bridge and the orientation of D-Phe[1] are not uniquely defined because of the lack of suitable experimental conformational constraitns accessible under our experimental conditions. Therefore, our conformational search protocols, resulted in β-sheet structures with both left- and right-handed disulfide bridge chiralities, and a wide range of center-to-center distances between the aromatic rings of D-Phe[1] and Phe[3] (6−12 Å) can be accessed by β-sheet conformations. Within the β-sheet family, a conformation is accessible in which the D-Phe[1] side chain is in close proximity to the disulfide bridge (see arrow in Figure 3b, top) as also observed in the X-ray structure I (Figure 3b, bottom). The close proximity between the disulfide bridge and the D-Phe[1] side chain found in the X-ray structure I is maintained during 500 ps molecular dynamics at 300 K (Figure 4a), leading to a center-to-center distance between the aromatic rings of D-Phe[1] and Phe[3] in the range 12−14 Å. Combining this result with the previous conformational search, we conclude that the center-to-center distances between the aromatic rings of D-Phe[1] and Phe[3] in the β-sheet family span the range 6−14 Å. Therefore, not all the structures of the β-sheet group are consistent with the previously proposed model for μ-opioid antagonists, but β-sheet conformations are accessible which fulfill the pharmacophore topographical requirements for μ-opioid antagonism.

We also investigated the consistency of the helical structures with the model for high μ-opioid receptor affinity of sandostatin-based antagonists. In this regard, it is interesting to note that, as in the X-ray structure of molecule I, the proximity between the disulfide bridge and the D-Phe[1] side chain is also found in molecules II and III of sandostatin

crystals (Pohl et al., 1995). However, when molecular dynamics are simulated starting from the minimized X-ray structures of molecules III, the side chain of D-Phe[1] moves far from the disulfide bridge and close to the Phe[3] side chain (Figure 4b). Several molecular dynamics runs were also started from the minimized X-ray structure II (Pohl et al., 1995), generating an ensemble of conformations which includes structures with close D-Phe[1] and Phe[3] side chains.

On the basis of the molecular dynamics runs discussed above, the center-to-center distances between the aromatic rings of D-Phe[1] and Phe[3] in the helical ensemble span the interval 4−14 Å. This observation indicates that not all the structures of the helical ensemble fit the model for sandostatin-based μ-opioid antagonists, but helical conformations are accessible which are also consistent with the topographical requirements for μ-opioid antagonism, as also found in the case of the β-sheet family. However, the β-sheet group and the helical ensemble differ for the position of Thr[8] relative to the D-Phe[1] and Phe[3] aromatic pharmacophores (Figure 4). These conformational differences can be advantageously used in the design of conformationally constrained sandostatin peptidomimetics aimed at probing the biological relevance of the different orientations of Thr[8]. These studies are expected to provide further insight into the role of Thr[8] for which chemical modifications were shown to affect the binding to μ-opioid receptors (Pelton et al., 1985; Kazmierski et al., 1988).

SUMMARY AND CONCLUSIONS

Attempts to explain all NMR data on sandostatin in DMSO-d_6 solution using a single conformation lead to NOE violations and to discrepancies among the NOE-based structures, the $J_{HNC^{\alpha}H}$ based structures, and the structures derived from the temperature coefficients. These inconsistencies are solved if an equilibrium is assumed between antiparallel β-sheet structures and conformations in which the C-terminal residues fold into a 3_{10} helix-like array (helical ensemble). This conformational equilibrium is also consistent with previous X-ray investigations which show that the asymmetric unit of sandostatin crystals contains molecules characterized by the same β-sheet and helical secondary structure features found for sandostatin in DMSO-d_6 solution. In addition, the proposed conformational equilibrium also explains the NMR data of sandostatin acquired in a water/MeOH mixture including several mutually exclusive NOEs. These observations suggest that the conformational propensities revealed by our study in DMSO-d_6 reflect an intrinsic property of sandostatin detectable in different environments.

The present study provides a basis for the conformational characterization of other molecules related to sandostatin for which mutually exclusive NOEs are observed. For instance, D-Nal[1]-Cys[2]-Tyr[3]-D-Trp[4]-Lys[4]-Val[6]-Cys[7]-Thr[9]-NH_2 (disulfide bridged), a highly active somatostatin analog named DC13−116, shows the same sets of mutually exclusive NOE observed for sandostatin in DMSO-d_6 (Verheyden et al., 1990). A proper multiconformational characterization of these analogs is important in order to avoid conformational averaging artifacts. In this regard, the work reported here can be expanded using also other approaches to multiconformational NMR including MEDUSA (Bruschweiler et al., 1991; Blackledge et al., 1993) and other methods to model NMR data as ensemble averages (Kessler et al., 1988; Scheek et al., 1991; Nikiforovich et al., 1993; Mierke et al., 1994; Fennen et al., 1995).

Finally, this investigation offers a structural basis for the design of novel sandostatin-based peptidomimetics: accessible β-sheet structures fit the known model for somatostatin-like bioactivity, and subsets of both the β-sheet and the helical ensembles are consistent with the 7.5 Å center-to-center distance between the aromatic rings of D-Phe[1] and Phe[3] required for μ-opioid antagonistic activity. However, the position of Thr[8] relative to the aromatic pharmacophores is different in the β-sheet and in the helical structures. This difference can be used to design conformationally restricted sandostatin analogs expected to provide insight into the observed effects of Thr[8] on μ-opioid binding affinities.

ACKNOWLEDGMENT

We thank Sandoz for the generous gift of a sample of sandostatin. We thank also Prof. Sheldrick for providing the coordinate files of the X-ray-derived structures of sandostatin.

SUPPORTING INFORMATION AVAILABLE

Assignments of the proton chemical shifts and temperature coefficients of the NH resonances (1 page). Ordering information is given on any current masthead page.

REFERENCES

Arison, B. H., Hirschmann, R., & Veber, D. F. (1978) *Bioorg. Chem. 7*, 447.
Aue, W. P., Bartholdi, E., & Ernst, R. R. (1976) *J. Chem. Phys. 64*, 2229.
Baker, E. N., & Hubbard, R. E. (1984) *Prog. Biophys. Mol. Biol. 44*, 97.
Bauer, W., Briner, U., Doepfner, W., Haller, R., Huguenin, R., Merbach, P., Petcher, T. J., & Pless, J. (1982) *Life Sci. 31*, 1133.
Bax, A., & Davis, D. G. (1980) *J. Magn. Reson. 37*, 93.
Bax, A., & Freeman, R. (1981) *J. Magn. Reson. 44*, 542.
Blackledge, M. J., Bruschweiler, R., Griesinger, C., Schmidt, J. M., Xu, P., & Ernst, R. R. (1993) *Biochemistry 41*, 10960.
Bodenhausen, G., Vold, R. L., & Vold, R. R. (1980) *J. Magn. Reson. 37*, 93.
Bothner-By, A. A., Stephens, R. L., Lee, J., Warren, C. D., & Jeanloz, R. W. (1984) *J. Am. Chem. Soc. 106*, 811.
Brady, S. F., Paleveda, W. J., Arison, B. H., Saperstein, R., Brady, E. J., Raynor, K., Reisine, T., Veber, D. F., & Freidinger, R. M. (1993) *Tetrahedron 49*, 3449.
Bruschweiler, R., Blackledge, M., & Ernst, R. R. (1991) *J. Biomol. NMR 1*, 3.
Buffington, L., Garsky, V., Massiot, G., Rivier, J., & Gibbons, W. A. (1980) *Biochem. Biophys. Res. Commun. 93*, 376.
Bystrov, V. F. (1976) *Prog. Nucl. Magn. Reson. Spectrosc. 10*, 41.
Clore, G. M., Appella, E., Yamada, M., Matsushima, K., & Gronenborn, A. M. (1990) *Biochemistry 29*, 1689.
Cung, M. T., & Marraud, M. (1982) *Biopolymers 21*, 953.
Davis, D., & Bax, A. (1985) *J. Am. Chem. Soc. 107*, 2820.
Delfs, J. R., & Dichter, M. A. (1983) *J. Neurosci. 3*, 1176.
Fennen, J., Torda, A. E., & van Gunsteren, W. F. (1995) *J. Biomol. NMR 6*, 163.
Fesik, S. W., Gampe, R. T. J., Holzman, T. F., Egan, D. A., Edalji, R., Luly, J. R., Simmer, R., Helfrich, R., Kishore, V., & Rich, D. H. (1990) *Science 250*, 1406.
Fesik, S. W., Gampe, R. T. J., Eaton, H. L., Gemmecker, G., Olejniczak, E. G., Neri, P., Holzman, T. F., Egan, D. A., Edalji, R., Helfrich, R., Hochlowski, J., & Jackson, M. (1991) *Biochemistry 30*, 6574.
Gulya, K., Pelton, J. T., Hruby, V. J., & Yamamura, H. I. (1986) *Life Sci. 38*, 2221.
Hagler, A. T. (1985) in *Peptides* (Udenfriends, S., et al., Eds.) Vol. 7, pp 214−296, Academic Press, Orlando, FL.

Hallenga, K., Van Binst, G., Scarso, A., Michel, A., Knappenberg, M., Dremier, C., Brison, J., & Dirkx, J. (1980) *FEBS Lett. 119*, 47.
Hawkins, K. N., Knapp, R. J., Lui, G. K., Gulya, K., Kazmierski, W., Wan, Y. P., Pelton, J. T., Hruby, V. J., & Yamamura, H. I. (1989) *J. Pharmacol. Exp. Ther. 248*, 73.
He, Y. B., Huang, Z., Raynor, K., Reisine, T., & Goodman, M. (1993) *J. Am. Chem. Soc. 115*, 8066.
Huang, Z., He, Y.-B., Raynor, K., Tallent, M., Reisine, T., & Goodman, M. (1992) *J. Am. Chem. Soc. 114*, 9390.
Iverson, L. L. (1983) *Annu. Rev. Pharmacol. Toxicol. 23*, 1.
Levitt, M. H., Freeman, R., & Frenkiel, T. (1982) *J. Magn. Reson. 47*, 328.
Loosli, H. R., Kessler, H., Oschkinat, H., Weber, H. P., Petcher, T. J., & Widmer, T. J. (1985) *Helv. Chim. Acta 68*, 682.
Kaupmann, K., Bruns, C., Raulf, F., Weber, H. P., Mattes, H., & Lubbert, H. (1995) *EMBO J. 14*, 727.
Kazmierski, W., & Hruby, V. J. (1988) *Tetrahedron 44*, 697.
Kazmierski, W., Wire, W. S., Lui, G. K., Knapp, R. J., Shook, J. E., Burks, T. F., Yamamura, H. I., & Hruby, V. J. (1988) *J. Med. Chem. 31*, 2170.
Kazmierski, W., Yamamura, H. I., & Hruby, V. J. (1991) *J. Am. Chem. Soc. 113*, 2275.
Kazmierski, W., Ferguson, R. D., Knapp, R. J., Lui, G. K., Yamamura, H. I., & Hruby, V. J. (1992) *Int. J. Pept. Protein Res. 39*, 401.
Kazmierski, W., Ferguson, R. D., Lipkowski, A. W., & Hruby, V. J. (1995) *Int. J. Pept. Protein Res. 46*, 265.
Kessler, H. (1982) *Angew. Chem., Int. Ed. Engl. 21*, 512.
Kessler, H., Griesinger, C., Lautz, J., Muller, A., van Gunsteren, W. F., & Berendsen, H. J. C. (1988) *J. Am. Chem. Soc. 110*, 3393.
Kopple, K. D., Bhandary, K. K., Kartha, G., Wang. Y., & Parameswaran, K. N. (1986) *J. Am. Chem. Soc. 108*, 4637.
Kramer, T. H., Shook, J. E., Kazmierski, W., Ayers, E. A., Wire, W. S., Hruby, V. J., & Burks, T. F. (1989) *J. Pharmacol. Exp. Ther. 249*, 544.
Maurer, R. ,Gaehwiler, B. H., Buescher, H. H., Hill, R. C., & Roemer, D. (1982) *Proc. Natl. Acad. Sci. U.S.A. 79*, 4815.
McCammon, J. A., Wolynes, P. G., & Karplus, M. (1979) *Biochemistry 18*, 927.
Mierke, D. F., Kurtz, M., & Kessler, H. (1994) *J. Am. Chem. Soc. 116*, 1042.
Mierke, D. L., Schiller, P. W., & Goodman, M. (1990a) *Biopolymers 29*, 943.
Mierke, D. L., Said-Nejad, O. E., Schiller, P. W., & Goodman, M. (1990b) *Biopolymers 29*, 179.
Noggle, J. H., & Schirmer, R. E. (1971) *The Nuclear Overhauser Effect*, Academic Press, New York.
Pachler, K. G. P. (1964) *Spectrochim. Acta 20*, 581.
Pelton, J. T., Gulya, K., Hruby, V. J., Duckles, S. P., & Yamamura, H. I. (1985) *Proc. Natl. Acad. Sci. U.S.A. 82*, 236.
Pelton, J. T., Kazmierski, W., Gulya, K., Yamamura, H. I., & Hruby, V. J. (1986) *J. Med. Chem. 29*, 2370.
Pelton, J. T., Whalon, M., Cody, W. L., & Hruby, V. J. (1988) *Int. J. Pept. Protein Res. 31*, 109.
Pepermans, H., Tourwe', D.; Van Binst, G., Boelens, R., Scheek, R. M., Van Gunsteren, W. F., & Kaptein, R. (1988) *Biopolymers 27*, 323.
Pohl, E., Heine, A., Sheldrick, G. M., Dauter, Z., Wilson, K. S., Kallen, J., Huber, W., & Pfaffli, P. J. (1995) *Acta Crystallogr. D51*, 48.
Rance, M., Sorensen, O. W., Bodenhausen, G., Wagner, G., Ernst, R. R., & Wuthrich, K. (1984) *Biochem. Biophys. Res. Commun. 117*, 479.
Reichlin, R. (1983a) *N. Engl. J. Med. 309*, 1495.
Reichlin, R. (1983b) *N. Engl. J. Med. 309*, 1556.
Rivier, J., Brown, M., & Vale, W. (1975) *Biochem. Biophys. Res. Commun. 65*, 746.
Scheek, R. M., Torda, A. E., Kemmink, J., & van Gunsteren, W. F. (1991) in *Computational Aspects of the Study of Biological Macromolecules by Nuclear Magnetic Resonance Spectroscopy* (Hoch, J. C., et al., Eds.) pp 209−217, Plenum Press, New York, NY.
Schiller, P. W. (1988) *Biophys. Chem. 31* (1−2), 63.
Schiller, P. W., & Di Maio, J. (1982) *Nature 297*, 74.
Schiller, P. W., Weltrowska, G., Nguyen, T. M., Lumieux, C., Chung, N. N., Marsden, B. J., & Wilkes, B. C. (1991) *J. Med. Chem. 34*, 3125.
Schiller, P. W., Nguyen, T. M., Weltrowska, G., Wilkes, B. C., Marsden, B. J., Lumieux, C., & Chung, N. N. (1992) *Proc. Natl. Acad. Sci. U.S.A. 89*, 1187.
Seybold, V. S., Hylden, J. L. K., & Wilcox, G. L. (1982) *Peptides 3*, 49.
Shaka, B., & Freeman, R. (1983) *J. Magn. Reson. 51*, 169.
Shook, J. E., Pelton, J. T., Lemcke, P. K., Porreca, F., Hruby, V. J., & Bruks, T. F. (1987) *J. Pharmacol. Exp. Ther. 242*, 1.
Sugg, E. E., Tourwe, D. Kazmierski, W., Hruby, V. J., & Van Binst, G. (1988) *Int. J. Pept. Protein Res. 31*, 192.
Van Binst, G., & Tourwe, D. (1992) *Peptide Res. 5* (1), 8.
Veber, D. F., Holly, F. W., Palaveda, W. J., Nutt, R. F., Bergstrand, S. J., Torchia, M., Glitzer, M. W., Saperstein, R., & Hirschmann, R. (1978) *Proc. Natl. Acad. Sci. U.S.A. 75*, 2636.
Veber, D. F., Freidinger, R. M., Perlow, D. S., Palaveda, W. J., Jr., Holly, F. W., Strachan, R. G., Nutt, R. F., Arison, B. J., Homnick, C. Randall, W. C., Glitzer, M. S., Saperstein, R., & Hirschmann, R. (1981) *Nature 292*, 55.
Verheyden, P., Francq, W., Pepermans, H., & Van Binst, G. (1990) *Biopolymers 30*, 855.
Weber, C., Wider, G., von Freyberg, B., Traber, R., Braun, W., Widmer, H., & Wuthrich, K. (1991) *Biochemistry 30*, 6563.
Widmer, H., Widmer, A., & Braun, W. (1993) *J. Biomol. NMR 3*, 307.
Wuthrich, K. (1986) in *NMR of Proteins and Nucleic Acids*, Wiley, New York.
Wynants, C., Van Binst, G., & Loosli, H. R. (1985a) *Int. J. Pept. Protein Res. 25*, 608.
Wynants, C., Van Binst, G., & Loosli, H. R. (1985b) *Int. J. Pept. Protein Res. 25*, 615.
Wynants, C., Tourwe, D., Kazmierski, W., Hruby, V. J., & Van Binst, G. (1989) *Eur. J. Biochem. 185*, 371.
Yamazaki, T., Said-Nejad, O. E., Schiller, P. W., & Goodman, M. (1991a) *Biopolymers 31*, 877.
Yamazaki, T., Probstl, A., Schiller, P. W., & Goodman, M. (1991b) *Int. J. Pept. Protein Res. 37*, 364.
Yamazaki, T., Mierke, D. L., Said-Nejad, O. E., Felder, E. R., & Goodman, M. (1992) *Int. J. Pept. Protein Res. 39*, 161.
Zuiderweg, E. R. P., Boelens, R., & Kaptein, R. (1985) *Biopolymers 24*, 601.

BI962497O